ARTICLE

Hindered Water Motions in Hardened Cement Pastes Investigated over Broad Time and Length Scales

Heloisa N. Bordallo,*,† Laurence P. Aldridge,‡ Peter Fouquet,§ Luis Carlos Pardo,∥,⊥ Tobias Unruh,# Joachim Wuttke,⊥ and Fabiano Yokaichiya†

Helmholtz-Zentrum Berlin für Materialien und Energie GmbH, Glienicker Strasse 100, D-14109 Berlin, Germany, Institute of Materials Engineering, ANSTO, PMB 1 Menai, New South Wales 2234, Australia, Institut Laue Langevin, 6 rue Jules Horowitz, F-38042 Grenoble Cédex 9, France, Grupo de Caracterització de Materials, Departament de Física i Enginyeria Nuclear (ETSEIB), Universitat Politècnica de Catalunya, E-08028 Barcelona, Spain, Jülich Centre for Neutron Science at FRM II, Forschungszentrum Jülich GmbH, Institut für Festkörperforschung, Lichtenbergstrasse 1, D-85747 Garching, Germany, and Forschungsneutronenquelle Heinz Maier-Leibnitz and Physikdepartment E13, Technische Universität München, Lichtenbergstrasse 1, D-85747 Garching, Germany

ABSTRACT We investigated the dynamics of confined water in different hydrated cement pastes with minimized contributions of capillary water. It was found that the water motions are extremely reduced compared to those of bulk water. The onset of water mobility, which was modified by the local environment, was investigated with elastic temperature scans using the high-resolution neutron backscattering instrument SPHERES. Using a Cauchy−Lorenz distribution, the quasi-elastic signal observed in the spectra obtained by the backscattering spectrometer was analyzed, leading to the identification of rotational motions with relaxation times of 0.3 ns. Additionally, neutron spin echo (NSE) spectroscopy was used to measure the water diffusion over the local network of pores. The motions observed in the NSE time scale were characterized by diffusion constants ranging from 0.6 to 1.1 × 10^{-9} m^2 s^{-1} most likely related to water molecules removed from the interface. In summary, our results indicate that the local diffusion observed in the gel pores of hardened cement pastes is on the order of that found in deeply supercooled water. Finally, the importance of the magnetic properties of cement pastes were discussed in relation to the observation of a quasi-elastic signal on the dried sample spectra measured using the time-of-flight spectrometer.

KEYWORDS: cement paste • pore structure • neutron scattering • water dynamics • water diffusion • magnetic relaxation

INTRODUCTION

Concrete, the most abundant of the man-made materials, also predates both pottery and metal as the first industrially produced material (1). Over 8000 years ago, it was produced in half-ton lots. This hydraulic cement was produced from fired limestone that carbonated to give concrete with a compressive strength of greater than 30 MPa, which is similar to that of conventional construction concrete produced in ready-mix plants today. About 5000 years ago, the Egyptians heated gypsum to use as a cementitious material, and later, the Greeks developed a calcium silicate system, which was used by the Romans to produce concrete that has proven to be durable for over 2000 years. Today, Portland cement, a fired calcium silicate produced from the processing of limestone with clay, is normally used for concrete production. Portland cement generally has as the major component alite, the simplest form having the composition Ca_3SiO_5. The complete hydration reaction of this alite can be written (2) as $Ca_3SiO_5 + 5.3H_2O = Ca_{1.7}SiO_{3.7}\cdot 4H_2O + 1.3Ca(OH)_2$.

It must be understood that this reaction is only a gross approximation of the hydration of ordinary Portland cement (OPC) because it neglects aluminum, sulfur, potassium, and sodium, which all play an important role in cement hydration (3). A Portland cement clinker has at least four compounds. The composition depends on both impurities such as iron in the raw materials and the temperature of firing. The clinker is interground with gypsum, and the resulting cement reacts with water to produce a cement paste, the key component of which is amorphous calcium silicate hydrate designated as C−S−H. This C−S−H has a variable composition. For example, when cement is blended with pozzolanic materials containing reactive silica, then C−S−H has (2) a calcium/silicon ratio of 1.5 rather than 1.7. In this case, the reaction can be written as $Ca_3SiO_5 + SiO_2 + 7.6H_2O = 2Ca_{1.5}SiO_{3.5}\cdot 3.8H_2O$. Pozzolanic materials, such as ground granulated blast furnace slag (GGBFS), can be blended or interground with Portland cement to give a concrete that can have durability superior to that of normal concrete (3). Nokken et al. (4) show that the blast furnace

* Corresponding author. Tel: +49 (0)30 8062 2924. Fax: +49 (0)30 8062 2781. E-mail: bordallo@helmholtz-berlin.de.
Received for review May 15, 2009 and accepted September 3, 2009
† Helmholtz-Zentrum Berlin für Materialien und Energie GmbH.
‡ Institute of Materials Engineering, ANSTO. E-mail: laurie.aldridge@gmail.com.
§ Institut Laue Langevin.
∥ Universitat Politècnica de Catalunya.
⊥ Forschungszentrum Jülich GmbH.
Forschungsneutronenquelle Heinz Maier-Leibnitz.
DOI: 10.1021/am900332n

Published on Web 09/25/2009

slag in concrete leads to a greater reduction in chloride diffusion with time. Such a reduction in diffusion could be assumed to result from a modification to the C−S−H influencing water diffusivity.

The focus, in this study, is on the mobility of water in hydrated cement paste. This paste is the key component of concrete that is made from cement mixed with sand aggregate and water. In well-made concrete, it is the transmission of water through the cement paste that governs the mobility of water. The nature of the cement paste is both controversial and complex, with many details still not being understood. The current knowledge has been well described by Taylor (3). However, it must be realized that the role of water changes as cement hydrates. Before cement hardens, most, if not all, of the water is mobile, and after the initial set, the most mobile water will be confined in the so-called capillary pores defined to possess pore diameters greater than 10 nm (5). The Powers−Brownyard model (6), as set out in ref 7, quantifies the relationship between the hardening cement and the hydration products. Water transmission through concrete is critically dependent on the amount of capillary pores. The volume of the capillary pores decreases as the cement hydrates. In fact, in concrete made with a water-to-cement ratio (w/c) of about 0.45, the capillary pores in the cement paste are reported to become discontinuous after 7 days of hydration (8), and when this happens, the water transmission is controlled by the smaller gel pores, which by definition have pore diameters of less than 10 nm. It is considered by Taylor (3) that one-third of the water in the gel pores will be confined in an interlayer region of possibly about 1 nm, while the remainder of the gel pore water will be in fine pores of diameters up to 10 nm.

The cement paste is slow to harden, and Taylor (3) states that 70% of the alite component of the paste hydrates in 28 days. As cement hydrates, the water can be either (1) bound as hydroxyl in C−S−H, (2) mobile water in the capillary pores, or (3) confined in the gel pores with a significant fraction of this water confined in an interlayer similar to that found in clays. It is considered (2) that a completely hydrated paste of pure alite has the composition $Ca_{1.7}SiO_{3.7} \cdot 4H_2O$ with 1.2 mol of bound water and 2.8 mol of gel water, while a completely hydrated paste of pozzolanic cement would have the composition $Ca_{1.5}SiO_{3.5} \cdot 3.8H_2O$ with 1 mol of bound water and 2.8 mol of gel water. Parrot and co-workers (9) have measured the amount of hydration of three cements as a function of time and shown that at 28 days the cements were 51−81% hydrated while at 90 days the cements were 63−91% hydrated. If it is assumed that at 28 days 70% of the cement is hydrated and that at 90 days this value is 90%, by applying the Powers−Brownyard theory to compute the division of water between capillary pores, gel pores, and the bound state, we obtain the values given in Table 1. The details for the calculations are given in the Appendix.

From the above description, it can be concluded that the pore structure of the cement paste is complex and always developing as the cement hydrates and mobile water is chemically bound to the calcium silicate structure and constrained in the gel pores. As shown in Table 1, hydration can be considered to be a transformation of water from the larger capillary pores to being chemically bound as hydroxyls in the calcium silicate hydrates or physically bound in the gel pores. This concept of how water interacts with the pores is illustrated in Figure 1. The more mobile water is in the relatively large capillary pores, the more constrained water is in the gel pores, either in interlayer regions or in very fine pores with geometry similar to that of the capillary pores but with pore diameters of less than 10 nm. It should be noted that the division between the capillary and gel pores is not unambiguous, and some of the capillary water may be found in pores that can only be accessed through gel pores. Also indicated in Figure 1 are the amount of hydrogen split between hydroxyl groups found both in C−S−H and calcium hydroxide and in water in both the (largely empty) capillary pores and gel pores.

Table 1. Comparison between the Partition of Water in Marine and OPC Pastes at 70%, 90% or 100% Hydration[a]

paste	sample	reaction (%)	bound (%)	gel (%)	capillary (%)
Marine (w/c = 0.42)	1	70	21	58	21
		90	26	74	0
		100	26	74	0
OPC (w/c = 0.42)	4	70	33	37	30
		90	39	51	10
		100	43	56	1
OPC (w/c = 0.6)	6	70	23	26	51
		90	30	33	37
		100	33	37	30

[a] The samples used in this work are identified by the numbers given in the second column.

The ratio of bound to mobile water in hydrated cement has been measured using inelastic neutron scattering by Harris et al. (10), and this technique has been used in a number of studies to apportion bound and free water in pastes made from both pure alite and cement pastes. In earlier papers (11, 12) on cement paste, we have used quasi-elastic neutron scattering (QENS) to (1) differentiate between three different types of water, (a) chemically bound, (b) free, or (c) physically bound, (2) differentiate the water mobility at different time scales by using different energy resolutions (time scales), (3) show that when the paste is heated to 105 °C, all of the free and physically bound water was removed, and (4) show that the water adsorbed back onto the paste heated at 105 °C behaved like free water.

In a time where the effects of global warming on weather patterns is accepted as a real and serious problem and where the cement industry produces 5−7% of the world's carbon dioxide emission, decreasing the production of carbon dioxide is a crucial issue. Thus, it is important to improve the production of and develop more durable concretes that require less carbon dioxide. To reach such a goal, the knowledge of the physical chemistry of the water−cement paste interactions, which is fundamental in the understanding and prediction of the service life of the concrete infrastructure, must be expanded. The durability of concrete is

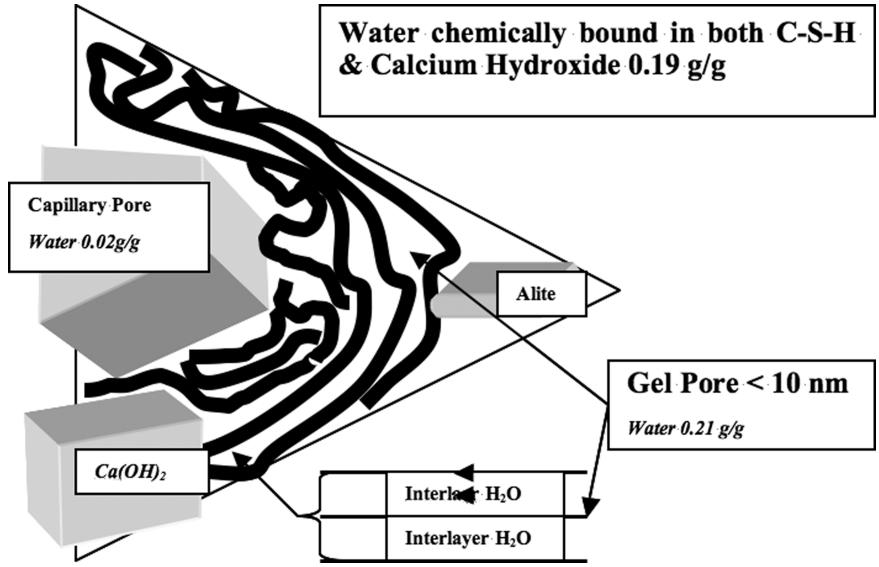

FIGURE 1. Water and its relationship to the microstructure of hydrated Portland cement paste. The amounts of water in the (mostly empty) capillary pore and gel pore have been calculated from the Powers−Brownyard model, assuming that 95% of the paste (made with w/c = 0.42) cement had been hydrated. When 1 g of cement is 95% hydrated, the unreacted products are 0.05 g of cement, 0.02 of water with reacted products C−S−H (0.65 g), and calcium hydroxide (0.40 g). The water is spilt between the bound water in C−S−H (0.09 g), bound water in calcium hydroxide (0.10 g), gel water (0.21 g), and capillary water (0.02 g). In the figure, C−S−H is represented by thick irregular lines with interlayer water confined between the layers. Note that the gel water is considered to be both in fine pores and in the interlayer.

related to its ability to limit fluid transmission, and knowledge of how to reduce the rate at which water will be transmitted through the cement paste is critical to achieving durability. Our motivation in this paper was to explore how far QENS may be used to differentiate between the capillary pore and gel water and to test the hypothesis, previously advanced, that the physically bound water was constrained in the gel pores while the free water was in the capillary pores. We also wanted to confirm that reabsorbed water was less constrained than the original water in the paste. The latter hypothesis was checked using elastic fixed-window scans, similar to those used to elucidate the mobility of water in clays (13), the glass transition in water (14), and the dynamics of water molecules in aqueous solutions confined silica matrixes (15). To differentiate water in the gel and capillary pores, we assumed that OPC paste cured over 100 days and made with a w/c ratio of 0.42 would have essentially no capillary water (16), while pastes made at w/c = 0.6 would have substantially more water in the capillary pores. Further differentiation of the w/c = 0.6 pastes could be made by drying the pastes in a CO_2-free atmosphere of relative humidity (RH) ~ 50% so that all of the water from the capillary pores is removed (6).

MATERIALS AND METHODS

Cement Samples. We used two types of cement samples: Marine cement, comprising 60% GGBFS interground with OPC and gypsum (samples 1−3), and pure OPC (samples 4−7). Both cements are commercial products and comprise the same basic Portland cement from Blue Circle Southern in Australia. The pastes were prepared by shear mixing with the required amount of tap water (17), and samples were cured in a sealed environment over 100 days. The cured samples used in the neutron experiments were confined in an aluminum container after being crushed, ground, and sealed inside aluminum foil to avoid any corrosion of the sample holder.

The preparation of the seven cement paste samples was as follows:

Sample 1: Marine paste with a w/c ratio of 0.42, which should have practically no capillary pore water.

Sample 2: Marine paste, the same as sample 1 but further processed by oven drying at 105 °C to constant weight. It is generally considered that, at 105 °C, the free water—evaporable water—is removed; thus, this sample should have only chemically bound water (18).

Sample 3: Marine paste, the same as sample 2 but further processed by introducing reabsorbed water. The sample was placed in a vacuum desiccator over a saturated salt solution of $Mg(NO_3)_2 \cdot 6H_2O$ with the air removed so that the atmosphere had a RH of 52%. This sample should have capillary and gel pore water, with the water located preferentially in the gel pores.

Sample 4: OPC paste made with a w/c ratio of 0.42, which should have practically no capillary pore water (16).

Sample 5: OPC paste, the same as sample 4 but further processed by oven drying at 105 °C to constant weight.

Sample 6: OPC paste made with a w/c ratio of 0.60, which would have both capillary and gel pore water.

Sample 7: OPC paste, the same as sample 6 but further dried for 4 days in a vacuum over a saturated salt solution having a RH (19) of 52%. This sample was not oven-dried and should have only gel water.

Neutron Scattering Measurements. We measured the elastic incoherent structure factor (EISF) using the SPHERES (20, 21) backscattering spectrometer of the JCNS (Jülich Center for Neutron Science) outstation at the FRM II (Forschungsneutronenquelle Heinz Maier-Leibnitz, Garching, Germany) in the temperature range of 4−300 K. Using an incident wavelength of 6.271 Å, the backscattering spectrometer provides an elastic energy resolution (ΔE) of 0.63 μeV (fwhm) covering motions in the range of a few nanoseconds in a Q range of 0.78 $Å^{-1} < Q <$ 1.8 $Å^{-1}$. In this configuration, if we define the confinement length scale, $\xi \approx \pi/Q$, the length scale where the dynamic slowing down manifests itself is about 5 Å at room temperature.

Time-of-flight (TOF) spectra on samples 2 and 5 (oven-dried Marine and OPC samples) were measured using the multichopper spectrometer TOFTOF (22), located at FRM II, using an incident wavelength of 6 Å, corresponding to an elastic energy

resolution ΔE of 65 μeV (fwhm), covering a Q range of 0.4 Å^{-1} $\leq Q \leq$ 1.8 Å^{-1}. The regions with Bragg reflections from the sample were excluded from data evaluation.

Additionally, the intermediate scattering function $I(Q,t)$ of samples 4, 6, and 7 was measured on the IN11 neutron spin−echo (NSE) spectrometer at ILL (Institut Laue Langevin, Grenoble, France) for Q values in the range of 0.37 Å^{-1} < Q < 1.71 Å^{-1} and for Fourier times 3 ps < t < 1 ns using an incident neutron wavelength of 5.5 Å. The data were collected at 300 K and corrected for instrumental resolution by normalizing each scan to the elastic reference scan with the same samples at 2 K.

Magnetic Measurements. Magnetic measurements were made using a SQUID magnetometer (Quantum Design MPMS), and the temperature dependence of the susceptibility was deduced. A typical sample mass was 100 mg.

RESULTS

Distinctive Properties of the Cement Pastes Reflected by the High-Resolution Inelastic Neutron Data. To better understand the dynamics observed in the time window covered by SPHERES, we carefully inspected the evolution of the EISF [$S(Q, \omega=0)$] as a function of the temperature for samples 1−3. This approach provides information on the geometry of atomic motions and can be expressed as the spatial Fourier transform of the long-time-limit self-correlation function (23), which evaluates the probability to find a particle around the position r at time t, knowing it was at $r = 0$ at $t = 0$. Thus, significant EISF values will only be detected if the atomic motions are space-restricted, a condition of water confined in cement pastes. Additionally, in the cement paste, the response of the H nuclei will dominate the signal because of their large cross section. Assuming that the Debye model is applicable, $\langle u^2 \rangle$ can be described by the Debye−Waller factor. Therefore, the data given in Figure 2, which have a summed Q range, were fitted by the following expression (24):

$$\langle u^2 \rangle = \frac{3\hbar^2 T}{m k_B \theta_D^2}\left[\Phi\left(\frac{\theta_D}{T}\right) + \frac{1}{4}\left(\frac{\theta_D}{T}\right)\right] \quad (1)$$

where $\hbar$ is the reduced Planck constant, T is the temperature, m represents the mass of the scatters, k_B is the Boltzmann constant, θ_D is the Debye temperature, and $\Phi(x)$ is the Debye integral.

As shown in Figure 2 and within the statistical accuracy of our data, in the measured time scale, the dry sample (sample 2) can be described by the harmonic model in the whole temperature, whereas for the Marine w/c = 0.42 (sample 1), nonharmonic contributions are evident above 230 K. For the Marine w/c = 0.42 rehydrated at 52% RH (sample 3), two crossover temperatures at 200 and 250 K are observed. The latter observation indicates that after rehydration the gel pores were filled and, consequently, the water is more mobile. Previous studies have shown that while bulk water can be supercooled to ∼260 K (25), water confined in micropores of 3 nm can be supercooled to ∼238 K and water confined in bigger pores of ∼10 nm can be supercooled to 253 K (26). Moreover, very recently (27), it

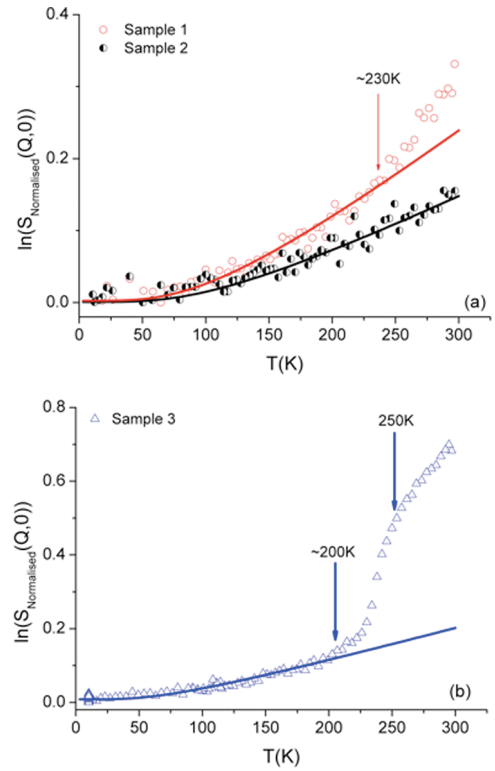

FIGURE 2. Comparison between the normalized $S_{inc}(Q,0)$ a function of the temperature between samples with w/c = 0.42. The data plotted in this figure have Q values ranging between 0.78 and 2 Å. The arrows indicate where the water motion is activated, with deviation from the linear decrease in a given temperature range.

was shown that in 30-day-old hydrated white cement an exothermic peak at about 230 K was observed and was attributed to water confined in the gel pores.

If we assume that we are dealing with true elastic (E) plus quasi-elastic (QE) scattering, the QE signal will account for motional disorder within the time range resolved by the experiment and imposed by individual physical parameters of the pore structure. Indeed, after subtraction of the signal due to the paste alone (dried sample), QE is clearly observed. By focusing on the analysis of the QE region of the spectrum obtained on SPHERES for the 100-day-cured Marine and OPC samples with w/c = 0.42 (samples 1 and 4), we can access the correlation times associated with the water mobility in both pastes. It is important to recall that the different distributions of the pore size create different surface water binding behavior and hence will generate different relaxation times. Such a distribution of relaxation times would give rise to a central narrow peak of approximately the width of the resolution function combined with a broad and yet significant tail. To minimize the number of required components and parameters in such a multifunction fit, this type of time distribution can be approximated by the Cauchy−Lorenz distribution (28, 29), $[(\omega/\Gamma_s)^2 + 1]^{-1}/\pi\Gamma_s$, where Γ_s is the half-width at half-maximum (hwhm) and which has the desired properties that enable us to fit the QE response with a delta line plus a Lorentzian function.

To analyze the data, the spectra were grouped into three groups with different Q values. The fitted result for sample

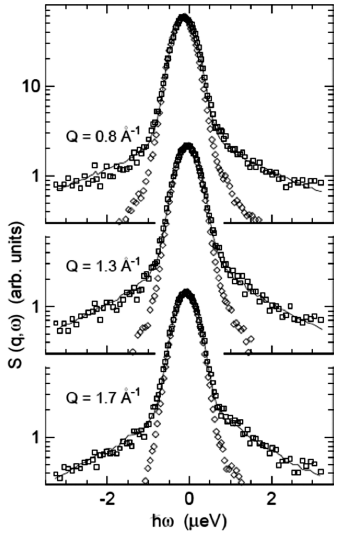

FIGURE 3. Experimental spectra (squares) at selected Q values for the OPC w/c = 0.42 (sample 4) measured at room temperature using SPHERES, $\Delta E = 0.63$ μeV. The best fit (solid line) was obtained using a Cauchy−Lorentz function plus an elastic component. The resolution function is shown as lozenges.

4 is given in Figure 3. For both samples, the fractional elastic contribution coming from the water molecules that are bound to the cement paste is on the order of 30%, in agreement with the Powers−Brownyard theory (see Table 1). The lack of Q dependence on the fitted hwhm ($\Gamma_s = 2.4 \pm 0.03$ μeV), for the samples with w/c = 0.42 (samples 1 and 3), seems to indicate that the protons are undergoing reorientational motions with a characteristic time of about 0.27 ns. This is in agreement with our previous work (11, 12) and similar to water observed in MCM-41 and MCM-48 matrixes (30), suggesting that these motions are almost sample-independent. Such dynamics can be related to motions in the interlayer space. In this region, strong bonds can be formed, resulting in a greater slowing down of the water molecules when compared to both bulk water and water confined in the bigger pores. Similar effects were observed by Nair et al. (31) in 3D nanoporous silicate layers spaced by claylike interlayer regions.

Translational Motions in the Gel Pores. Now we turn to the NSE spectra that measure the intermediate scattering function $I(\mathbf{Q},t)$ defined by the following equation as a function of the momentum transfer $\mathbf{Q}$ and Fourier time t.

$$I(Q,t) = N^{-1} \sum_{k,l} \langle e^{iQr_k(t)} e^{iQr_l(0)} \rangle \qquad (2)$$

where N is the number density, $r_{k,l}$ is the position of the scattering atom at time t, and Q is the wave vector. Considering that the vibrational, rotational, and translational motions are decoupled, $I(Q,t)$ can be expressed as $I_{inc}(\mathbf{Q},t) = I_{vib}(\mathbf{Q},t)\ I_{rot}(\mathbf{Q},t)\ I_{trans}(\mathbf{Q},t)$, The vibrational contribution [$I_{vib}(\mathbf{Q},t)$] can be neglected simply because the corresponding energy transfers are beyond the cutoff energy of the NSE spectrometer. Moreover, in the case of bulk and confined water for $Q < 1.0$ Å^{-1}, the contribution

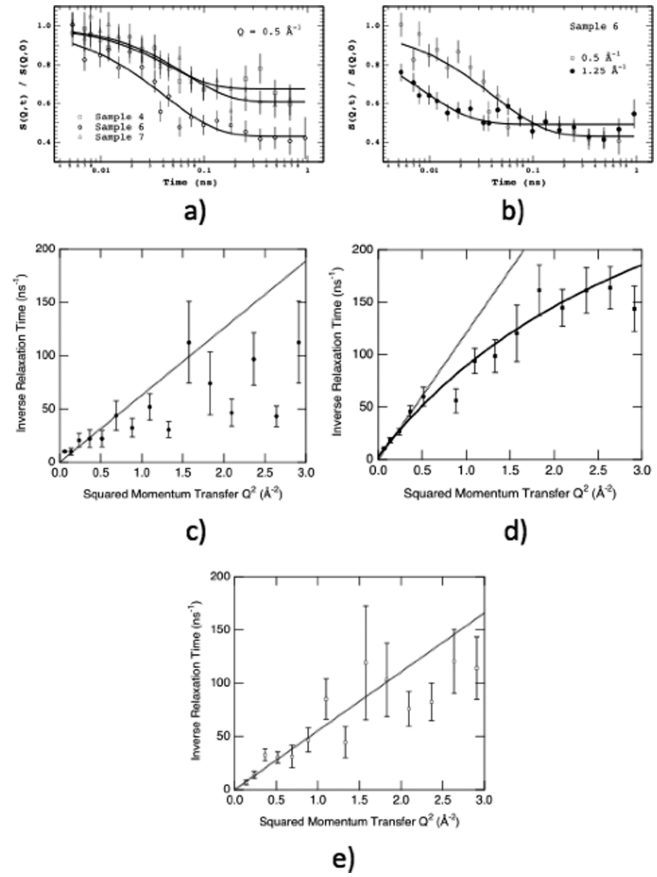

FIGURE 4. (a) Q-resolved $I(Q,t)$ scans of samples 4, 6, and 7 (OPC pastes with w/c = 0.42, 0.6, and 0.6 dried under controlled conditions) at $T = 300$ K for $Q = 0.5$ Å^{-1}. (b) $I(Q,t)$ scans of sample 6 (OPC paste with w/c = 0.6) for different Q values fitted with stretched exponential KWW functions (solid line). Fits of the experimental data with stretched exponential KWW functions (solid line) are also shown. Inverse relaxation time $\Delta E = \hbar/\langle\tau\rangle$ as a function of Q^2 obtained from the NSE data using the KWW stretched exponential function for samples 4 (c), 6 (d), and 7 (e). The solid lines are fits to the data using the jump diffusion model.

of the rotation of the H atoms around their center of mass [$I_{rot}(\mathbf{Q},t)$] can also be neglected. Therefore, at low-Q's, NSE gives information only on the translational motion.

Through a time-frequency Fourier transform of $I(Q,t)$, it is possible to calculate $S(Q,\omega)$. As a first phenomenological description, we may use the Kohlrausch−Williams−Watts (KWW) or stretched exponential function to parametrize the translational contribution (13):

$$I(Q,t) = \frac{S(Q,t)}{S(Q,t)} = [1 - A] \exp\left(-\frac{t}{\tau}\right)^{\beta} + A \qquad (3)$$

where τ is the typical relaxation time, β a stretching parameter (32), and A is the value of $I(Q,t)$ at long times. A finite value of A reflects a contribution of elastic scattering or motions that are too slow to appear in the dynamic window of the NSE spectrometer.

Q-resolved $I(Q,t)$ scans of OPC pastes (samples 4, 6, and 7) are presented in Figure 4. As shown in Figure 4a, the plots differ from those of hectorite (33) but are similar to those in hydrated sodium vermiculite (34). The KWW functional form

Table 2. Parameters Characterizing the Translational Motion of Water in Various Cement Pastes with w/c = 0.42, 0.6, and 0.6 Dried under Controlled Conditions at $T = 300$ K Using IN11[a]

sample	% immobile water	L (Å)	τ_0 (ps)	D_t (10^{-9}m^2/s)
bulk water(52)		1.53	1.57 ± 0.12	2.49 ± 0.07
OPC w/c = 0.42 (sample 4)	*30*−25			0.6 ± 0.1
OPC w/c = 0.6 (sample 6)	45	1.82 ± 0.05	2.4 ± 0.7	1.1 ± 0.1
OPC w/c = 0.6 at 52% RH (sample 7)	35			0.6 ± 0.1

[a] The percentage of mobile water observed in the time scale of this experiment is estimated from the NSE data by eq 3 or from the level of $I(Q,t)$ at long times [$I(Q,t=\infty) = A$], which correspond to the hydrogen of the structure or the immobile hydrogen in the time scale of the experiment, which is also given. Values of bulk water are given for comparison. Note that for the w/c = 0.42 this value was equally obtained from the SPHERES data, given in italic.

accurately describes all of the experimental spectra with a single stretching parameter β value of 0.85 (±0.15), indicating that the motion is mostly diffusive, except for the highest Q value for the OPC sample with w/c = 0.6 (sample 6). The overall high value of β reflects the narrow distribution of relaxation times. For all samples, the immobile fraction, A, is almost constant over the measured Q range.

The Q^2 dependence of the QE broadening, obtained from the typical relaxation time of the KWW fits, is shown in Figure 4c−e. For a continuous isotropic translational diffusion, a constant slope of the plot $1/\tau$ vs Q^2 is expected and $1/\tau = D_tQ^2$, where D_t in the latter equation is the long-range diffusion constant. The leveling off of the curve at high Q, $Q > 1$ Å^{-1} observed for the sample with w/c = 0.6 (sample 6), indicates jump rather than continuous diffusion, and in this particular case, we were able to describe the variation of $1/\tau$ vs Q approximately by the jump diffusion model of Singwi and Sjölander (35, 36). For samples 4 and 7, the Q dependence is not conventional and is not in good agreement with any model for translational jump diffusion; thus, we considered only the behavior observed at very low Q, as indicated by the dashed lines in the figure. The fitted parameters, characterizing the translational motions of unbound water as well as the fraction of bound water, are given in Table 2. The diffusion constant, D, and the residence time, τ_0, obtained from the analysis of our data are in good agreement with observations of the diffusion motion of water in other confined systems at room temperature (37, 38). In particular, we note that the translational diffusion of water in the hydrated cement paste, which was cured for over 100 days, is very similar to the values reported for the interlayer water in clays (13) but slower than the values reported for samples that were cured for 28 days. This would be expected if the water was confined to the gel pores.

Moreover, the amount of immobile hydrogen, given by the parameter A reported in Table 2, observed for sample 4 of about 25% for NSE and of about 30% for backscattering measurements agrees with the minimum value given in Table 1. It is worth noting that in our earlier work (11, 12) on 28-day-old samples (where ∼70% of the paste would be hydrated) we expected to have only about 30% of the bound water in OPC w/c = 0.42; however, in the time scales of the previous experiments, about 80% of the water was seen as immobile. The increased resolution of the NSE measurements, together with the improved background of the backscattering instrument, resolves the previous discrepancy.

Free Water in Pastes Heated at 105 °C? In the SPHERES and NSE data presented above as well as in our earlier work (11, 12) using the TOF spectrometer NEAT (BENSC, Berlin) and the backscattering HFBS (NIST, Washington, DC), no QE broadening was detected within the instrumental resolution; i.e., the signal is purely elastic in samples heated at 105 °C. Thus, we assumed, as is generally accepted (18), that after heating cement pastes at 105 °C only the surface hydroxyls remained, and if water molecules remain, they are fixed to the surface. This assumption was further supported by the earlier QENS studies of Hall et al. (39) on the dynamics of interlayer water in clays and by the recent work of Takahara et al. in MCM-41 (40). In spite of this and as shown in Figure 5, the measurements carried out using the TOF spectrometer TOFTOF do show a very tiny QE broadening, which could be fitted using a phenomenological expression described by one elastic peak plus one Lorentzian function. The hwhm's of the Lorentzian functions yield a relaxation time of about 3 ps.

To interpret such an observation, we must consider two scenarios: (1) Even after heating at 105 °C, a small amount of water may still be confined in the cement. (2) The system may have enough magnetic correlations to show diffusive fluctuations, giving rise to a QE broadening (41, 42). Even if both hypotheses may be true hereafter, we will only consider the magnetic behavior. It is important to recall that magnetic behavior in cement pastes was found to exist; see ref 43 and 44, which will, in turn, give rise to characteristic relaxation times that will influence part of the QE dispersion curve (13, 45). As demonstrated by Hansen et al. (45) in nanocrystalline hematite for temperatures where the thermal energy is comparable to or larger than the magnetic anisotropy energy, the magnetic relaxation time is in the picosecond range, which corresponds quite well with the domain of sensitivity of neutron scattering, which is also sensitive to magnetic relaxation. Therefore, we measured the magnetic susceptibility in three different cement pastes: a white Aalborg cement (produced from extremely pure limestone and sand with extremely low iron contents), the Berrima OPC, and a Marine paste containing GGBFS. The resulting magnetic susceptibilities are shown in Figure 5b. Bulk characterization of a white Aalborg cement and of the Berrima OPC shows essentially identical behavior that is typical of paramagnetic systems. Nearly all Portland cements contain iron, typically 0.5−5%, almost certainly contained

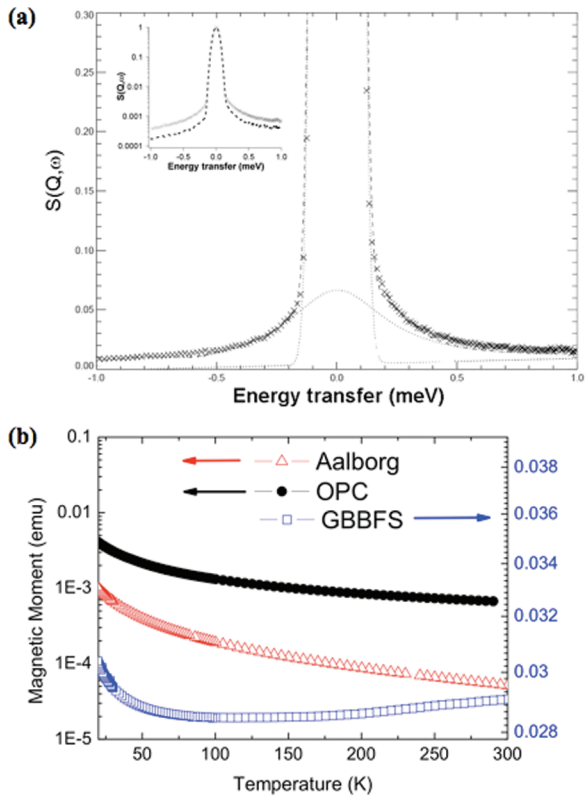

FIGURE 5. (a) Experimental QENS spectrum obtained using TOFTOF at FRM II ($\lambda = 6$ Å, $\Delta E = 65$ μeV, fwhm, $\langle Q \rangle = 1.1$ Å^{-1}) recorded from the dried 100-day-old OPC w/c = 0.42 (sample 5, crosses) compared to the fitted curve using a phenomenological model, described in the text. The inset shows the normalized neutron TOF spectra (crosses) compared to the resolution function (dotted line). (b) Mass susceptibility versus temperature of Aalborg (red triangles), OPC (black circle), GBBFS (blue squares) cement pastes measured in 1 kOe.

in Brownmillarite, $Ca_2Al_xFe_{2-x}0_5$ (43). Moreover, as observed by Kim et al. (43) in $Ca_2Al_xFe_{2-x}0_5$ and by Bordallo et al. (13) in natural clays, the amount of ferromagnetic Fe^{3+} in the crystalline lattice is not sufficient to exceed the percolation threshold, and therefore no long-range magnetic ordering occurs. Furthermore, the Aalborg white cement has a very low Brownmillarite content (46), explaining its smaller paramagnetic contribution. On the other hand, blast furnace slag generally contains more iron compounds than cement, and the Marine blend of cement used had 60% of the cement replaced by GGBFS. Thus, the magnetic parameters in the pastes made with this blend would be expected to be somewhat different from those made from OPC pastes. In fact, the magnetic parameters drop around room temperature and are similar to observations in pure, well-crystalline hematite (47, 48), which presents the so-called Morin transition around −10 °C (263 K). Thus, the magnetic parameters confirm that the iron content varies from paste to paste, and we are now investigating this interesting phenomenon.

In conclusion, as previously demonstrated in clays (13) and in a number of molecular magnets (49−51), magnetic fluctuations induced by the presence of magnetic ions in the lattice also lead to a QE broadening of the neutron spectra in the cement pastes. Thus, care should be taken when analyzing the data: basically the magnetic neutron scattering cross section of a single magnetic ion and the component characterizing the scattering law for water diffusion contribute significantly to the QE signal in the same Q region.

DISCUSSION AND CONCLUSION

In this work, we extended the dynamic range of earlier observations (11, 12), although we have observed less mobile water (or less signal) due to the longer curing times, by extending the time range of our observations and by carrying out our measurements on instruments with improved backgrounds, we were able to access more information. In concrete, pore water is confined to display a restriction of motion by at least 1 order of magnitude when compared to bulk water. In addition, we found different types of confined water within the water ensemble, thereby complicating the analysis of the dynamic response. However, by combining different techniques, we were able to extend our previous studies of water mobility in hardened cement pastes (11, 12) from a few nanoseconds to tenths of picoseconds. Furthermore, by curing longer, we used cement chemistry to minimize the contribution of the capillary pore water. Complementary information on the different water motions could be accessed within the range accessible in our neutron scattering measurements and were related to distinct dynamic processes. The process observed at the picosecond time scale is related to translational jumps of hydrogen-bonded water molecules. In contrast, reorientation motions, with characteristic times slightly below nanoseconds, can be related to a time-dependent reorientation of the water molecules that interact with the cement−paste interface. The lack of a Q dependence of this motion indicated that there is only a very limited diffusion involving these water molecules.

In summary, the results presented here show the following:

(1) Water that is reabsorbed into the cement paste is definitely more mobile than water in the "as-cured" samples. This suggests that the reabsorbed water is initially in the capillary pore and will take time to be admitted to the gel pores.

(2) Marine and OPC pastes (samples 1 and 4) with a w/c ratio of 0.42 show reorientation motions with characteristic times of about 0.27 ns that may be related to motion in the interlayer space.

(3) At the time scale of the NSE (nanoseconds to a few picoseconds), we observe the amount of immobile protons that is expected from the Powers−Brownyard model.

(4) Jump diffusion is observed in the OPC pastes with w/c = 0.6 (sample 6), while translational diffusion is observed when capillary pore water is reduced by drying of the paste in a 52% RH atmosphere (sample 7).

(5) The long-range diffusion constant, D_t, obtained for samples 4 and 7, which practically contain only gel pore water, is similar but reduced when compared to that of sample 6, which has both capillary and gel pore water.

(6) Finally, in addition to the QE scattering from water, there is another contribution to the observed spectra that comes from magnetic components of the cementitious matrix. It is important to separate the magnetic and water

contributions, and to do this in cement paste, we use the dried sample as the background.

It can be concluded that different motions of water in capillary or gel pores can be monitored; by using a combination of cement pastes; cured at different times, dried or cured at different RH, and examined by neutron scattering spectroscopy at different time (space) scales. Thus, neutron scattering gives cement chemists a powerful tool that can quantify the water motion in gel pores, allowing an understanding of the water−cement paste interaction at the molecular level. Such interactions control some of the most important macroproperties of concrete. Thus, neutron scattering may eventually prove to be as valuable as the water and nitrogen adsorption techniques to understand this amorphous, complex, and extremely valuable construction material.

APPENDIX

This appendix details the reactions to calculate the water partition given in Table 1. For OPC paste, it is assumed that $Ca_3SiO_5 + 5.3H_2O = Ca_{1.7}SiO_{3.7}\cdot 4H_2O + 1.3Ca(OH)_2$, where 1.2 mol of the water is bound to the calcium silicate and 2.8 mol of the water exists in the gel pores associated with C−S−H. In the equations given in this Appendix, the cement notation used is C=CaO, S = SiO_2, and H = H_2O. Note that excess unreacted water and alite are on the right-hand side of the equation. For Marine paste, it is assumed that the blend consists of an approximate composition of $Ca_3SiO_5 + SiO_2$. The chemical reaction is assumed to be $0.5(Ca_3SiO_5 + SiO_2) + 3.8H_2O = Ca_{1.5}SiO_{3.5}\cdot 3.8H_2O$, where 1 mol of the water is bound to the calcium silicate and 2.8 mol of the water exists in the gel pores associated with C−S−H.

(1) Reaction of OPC paste when w/c = 0.42:

70% reaction $C_3S + 5.3H = 0.7C_{1.7}SH_4 + 0.9CH + 0.3C_3S + 1.6H$

90% reaction $C_3S + 5.3H = 0.9C_{1.7}SH_4 + 1.2CH + 0.1C_3S + 0.5H$

100% reaction $C_3S + 5.3H = 1.0C_{1.7}SH_4 + 1.3CH + 0.0C_3S + 0.0H$

(2) Reaction of OPC paste when w/c = 0.60:

70% reaction $C_3S + 7.6H = 0.7C_{1.7}SH_4 + 0.9CH + 0.3C_3S + 3.9H$

90% reaction $C_3S + 7.6H = 0.9C_{1.7}SH_4 + 1.2CH + 0.1C_3S + 2.8H$

100% reaction $C_3S + 7.6H = 1.0C_{1.7}SH_4 + 1.3CH + 0.0C_3S + 2.3H$

(3) Reaction of Marine paste when w/c = 0.42:

70% reaction $\{0.5(C_3S + S) + 3.4H = 0.7C_{1.5}SH_{3.8} + 0.15(C_3S + S)\} + 0.7H$

90% reaction $\{0.5(C_3S + S) + 3.4H = 0.9C_{1.5}SH_{3.8} + 0.05(C_3S + S)\} + 0.0H$

100% reaction $\{0.5(C_3S + S) + 3.4H = 0.9C_{1.5}SH_{3.8} + 0.05(C_3S + S)\} + 0.0H$

(4) Reaction of Marine paste when w/c = 0.60:

70% reaction $0.5(C_3S + S) + 4.8H = 0.7C_{1.5}SH_{3.8} + 0.15(C_3S + S)\} + 2.1H$

90% reaction $0.5(C_3S + S) + 4.8H = 0.9C_{1.5}SH_{3.8} + 0.05(C_3S + S)\} + 1.4H$

100% reaction $0.5(C_3S + S) + 4.8H = 1.0C_{1.5}SH_{3.8} + 0.00(C_3S + S)\} + 1.0H$

Acknowledgment. The magnetic measurements were made using the facilities at the Laboratory for Magnetic Measurements at BENSC (LaMMB - MagLab). H.N.B. and L.P.A. thank M. Maccarini for help during the IN11 experiments. H.N.B. especially thanks M.-C. Bellissent Funel and C. Pappas for discussions on the analysis of the QE and NSE data and is also thankful for the financial support given through the ILL to perform the IN11 experiment. L.P.A. acknowledges traveling support funding from D. H. Aldridge. We gratefully acknowledge Michael Prager for the inspiration he gave to this work.

REFERENCES AND NOTES

(1) Kanare, H. *Concr. Constr. Mag.* **2009**, 1–15.
(2) Young, J. F.; Hansen, W. Volume relationships for C−S−H formation based on hydration stoichiometries. In *Microstructural Development during Hydration of Cement*; Struble, L. J., Brown, P. W., Eds.; Materials Research Society: Warrendale, PA, 1987; Vol. 85, pp 313−322.
(3) Taylor, H. F. W. In *Cement Chemistry*, 2nd ed.; Thomas Telford Publishing: London, 1997.
(4) Nokken, M.; Boddy, A.; Hooton, R. D.; Thomas, M. D. A. *Cem. Concr. Res.* **2006**, *36*, 200–207.
(5) Mindess, S.; Young, J. F.; Darwin, D. *Concrete*, 2nd ed.; Prentice Hall: Upper Saddle River, NJ, 2002.

(6) Powers, T. C., Brownyard, T. L. *Bulletin 22, Research Laboratories of the Portland Cement Association, Studies of the physical properties of hardened portland cement paste*; Portland Cement Association: Chicago, IL, 1948.
(7) Jensen, O. M.; Hansen, P. F. *Cem. Concr. Res.* **2001**, *31*, 647–654.
(8) Powers, T. C.; Copeland, L. E.; Mann, H. W. *J. PCA Res. Dev. Lab.* **1959**, *1*, 38.
(9) Parrott, L. J.; Geiker, M.; Gutteridge, W. A.; Killoh, D. *Cem. Concr. Res.* **1990**, *20*, 919–926.
(10) Harris, D. H. C.; Windsor, C. G.; Lawrence, C. D. *Mag. Concr. Res.* **1974**, *26*, 65–72.
(11) Bordallo, H. N.; Aldridge, L. P.; Desmedt, A. *J. Phys. Chem. B* **2006**, *110*, 17966–17976.
(12) Aldridge, L. P.; Bordallo, H. N.; Desmedt, A. *Phys. B* **2004**, *350*, E565−E568.
(13) Bordallo, H. N.; Aldridge, L. P.; Churchman, G. J.; Gates, W. P.; Telling, M. T. F.; Kiefer, K.; Fouquet, P.; Seydel, T.; Kimber, S. A. J. *J. Phys. Chem. C* **2008**, *112*, 13982–13991.
(14) Geila, B.; Koza, M. M.; Fujara, F.; Schober, H.; Natali, F. *Phys. Chem. Chem. Phys.* **2004**, *4*, 677–679.
(15) Mamontov, E.; Cole, D. R.; Dai, S.; Pawel, M. D.; Liang, C. D.; Jenkins, T.; Gasparovic, G.; Kintzel, E. *Chem. Phys.* **2008**, *352*, 117–124.
(16) Halperin, W. P.; Jehng, J-.Y.; Song, Y-.Q. *Magn. Res. Imaging* **1994**, *12*, 169–173.
(17) Although we did think long and hard about using demineralized or distilled water, we could see no benefits because the pore water in the paste will incorporate any soluble impurity that can be dissolved from the cement. For example, in low alkali cements, it is expected that a 0.2 M potassium ion will be found (pH ∼ 13), while with high alkali cements, the potassium ion is expected to be greater that 0.5 M (pH > 13.5), as is the case with calcium sulfate ions. Thus, pure water becomes quickly contaminated as ions dissolve from the cement during the "induction period of mixing". Hence, it was decided to use standard conditions for these experiments and always use Sydney Tap water as the mixing water.
(18) Gallé, C. *Cem. Concr. Res.* **2001**, *31*, 1467–1477.
(19) It has been considered that capillary pore water can be removed from cement pastes by drying the paste in a CO_2-free atmosphere with a RH of about 50%; thus, the same procedure was followed here.
(20) http://www.jcns.info/jcns_spheres.
(21) Wuttke, J.; Schneider, G. J.; Pardo, L. C. submitted for publication.
(22) Unruh, T.; Neuhaus, J.; Petry, W. *Nucl. Instrum. Methods* **2007**, *A 580*, 1414–1422.
(23) Borsali, R., Pecora, R., Eds. *Soft-Matter Characterization*; Springer: Berlin, 2008.
(24) Willis, B. T. M.; Pryor, A. W. In *Thermal Vibrations in Crystallography*; Cambridge University Press: Cambridge, U.K., 1975.
(25) Teixeira, J.; Bellisent-Funel, M.-C.; Chen, S.-H.; Dianoux, A. J. *Phys. Rev. A* **1985**, *31*, 1913–1917.
(26) Takamuku, T.; Yamagami, M.; Wakita, H.; Masuda, Y.; Yamaguchi, T. *J. Phys. Chem. B* **1997**, *101*, 5730–5739.
(27) Ridi, F.; Luciani, P.; Fratini, E.; Baglioni, P. *J. Phys. Chem. B* **2009**, *113*, 3080–3087.
(28) Brown, R. J. S.; Fantazzini, P. *Phys. Rev. B* **1993**, *47*, 14823–14834.
(29) Borgia, G. C.; Brown, R. J. S.; Fantazzini, P. *Phys. Rev. E* **1995**, *51*, 2104–2114.
(30) Liu, L.; Faraone, A.; Mou, C.-Y.; Yen, C.-W.; Chen, S.-H. *J. Phys.: Condens. Matter* **2004**, *16*, S5403–S5436.
(31) Nair, S.; Chowdhuri, Z.; Peral, I.; Neumann, D.; Dickinson, L. C.; Tompsett, G.; Jeong, H.-K.; Tsapatsis, M. *Phys. Rev. B* **2005**, *71*, 104301(8).
(32) The deviation of β from unity would indicate that the dynamics observed has a wide distribution of relaxation times.
(33) Marry, V.; Malikova, N.; Cadène, A.; Dubois, E.; Durand-Vidal, S.; Turq, P.; Breu, J.; Longeville, S.; Zanotti, J.-M. *J. Phys.: Condens. Matter* **2008**, *20*, 104205–104215.
(34) Swenson, J.; Bergman, R.; Longeville, S. *J. Chem. Phys.* **2001**, *115*, 11299–11305.
(35) Beé, M. *Quasi-Elastic Neutron Scattering*; Adam Hilger: Bristol, PA, 1988.
(36) Singwi, K. S.; Sjölander, A. *Phys. Rev.* **1960**, *119*, 863–871.
(37) Tuck, J. J.; Hall, P. L.; Hayes, M. H. B.; Ross, D. K.; Poinsignon, C. *J. Chem. Soc., Faraday Trans.* **1984**, *80*, 309–324.
(38) Swenson, J.; Bergman, R.; Howells, W. S. *J. Chem. Phys.* **2000**, *113*, 2873–2879.
(39) Hall, P. L.; Ross, D. K.; Tuck, J. J.; Hayes, M. H. B. *Proceedings of the IAEA Symposium on Neutron Inelastic Scattering—International Atomic Energy Agency*, Vienna, Oct 17−21, 1977; Vol. 1, p 617.
(40) Takahara, S.; Sumiyama, N.; Kittaka, S.; Yamaguchi, T.; Bellissent-Funel, M.-C. *J. Phys. Chem. B* **2005**, *109*, 11231–11239.
(41) Ersez, T.; Kennedy, S. J.; Finlayson, T. R. *Appl. Phys. A: Mater. Sci. Process.* **2002**, *74*, S725–S727.
(42) Gazeau, F.; Dubois, E.; Hennion, M.; Perzynski, R.; Raikher, Yu. *Europhys. Lett.* **1997**, *40*, 575–580.
(43) Kim, G. Y.; Roh, K. S.; Yo, C. H. *Bull. Korean Chem. Soc.* **1995**, *16*, 934–938.
(44) Jackson, M.; Sagnotti, L.; Rochette, P.; Sølheid, P. *IRM Quarterly* **2003**, *13*, 1.
(45) Hansen, M. F.; Bødker, F.; Mørup, S.; Lefmann, K.; Clausen, K. N.; Lindgård, P.-A. *Phys. Rev. Lett.* **1997**, *79*, 4910–4913.
(46) Bye, G. C. *Portland cement: Composition, production and properties*; Thomas Telford Publishing: London, 1999; Vol. 5, pp 164−165.
(47) Morin, F. J. *Phys. Rev.* **1950**, *8*, 819–820.
(48) de Boer, C. B.; Mullender, T. A. T.; Dekkers, M. J. *Geophys. J. Int.* **2001**, *146*, 201–216.
(49) Bordallo, H. N.; Chapon, L. C.; Cook, J. C.; Copley, J. R. D.; Goremychkin, E.; Kern, S.; Lee, S.-H.; Yildirim, T.; Manson, J. L. *Appl. Phys. A: Mater. Sci. Process.* **2002**, *74*, S634–S636.
(50) Bordallo, H. N.; Chapon, L.; Manson, J. L.; Hernandez-Velasco, J.; Ravot, D.; Reiff, W. M.; Argyriou, D. N. *Phys. Rev. B* **2004**, *69*, 224405(9).
(51) Garlea, V. O.; Nagler, S. E.; Zarestky, J. L.; Stassis, C.; Vaknin, D.; Kogerler, P.; McMorrow, D. F.; Niedermayer, C.; Tennant, D. A.; Lake, B.; Qiu, Y.; Exler, M.; Schnack, J.; Luban, M. *Phys. Rev. B* **2006**, *73*, 024414(5) .
(52) Bordallo, H. N.; Herwig, K. W.; Luther, B. M.; Levinger, N. E. *J. Chem. Phys.* **2004**, *121*, 12457–12464.

AM900332N